Research Paper
Computational Methods for Differential Equations
http://cmde.tabrizu.ac.ir
Vol. *, No. *, *, pp. 1-20
DOI:10.22034/cmde.2026.69117.3397

High-accuracy spectral volume reconstructions with Maximum-Principle-Satisfying and Positivity-Preserving properties for hyperbolic problems

Javad Farzi*
Department of Mathematics, Faculty of Basic Sciences, Sahand University of Technology, Sahand New Town, Tabriz, Iran.

Abstract

This paper presents the limited reconstruction of high-order spectral volume (SV) methods that rigorously satisfy the maximum principle and preserve positivity for scalar hyperbolic conservation laws and the compressible Euler equations, respectively. Standard high-order numerical methods often violate these physical constraints at the discrete level, leading to nonphysical oscillations and solutions—such as negative density or pressure. To address this, we introduce carefully designed limiter functions that modify the SV reconstruction polynomials within each cell while maintaining the scheme's high-order accuracy. This approach enforces the maximum-principle-preserving (MPP) and positivity-preserving (PP) properties in the numerical solution. A set of numerical tests shows that the method produces accurate, stable results for both smooth and discontinuous problems, confirming its high resolution and robustness.

Keywords. Maximum principle preserving, Positivity-preserving, Spectral volume schemes, Hyperbolic conservation laws, Compressible Euler systems, High order schemes.

2010 Mathematics Subject Classification. 65L20; 35L65.

1. Introduction

The focus of this paper is the development of high-order spectral volume (SV) schemes that satisfy the discrete maximum principle and preserve positivity in the numerical solution of hyperbolic conservation laws. Specifically, we consider the following one-dimensional scalar hyperbolic conservation law:

$$u_t + f(u)_x = 0, \qquad u(x,0) = u_0(x), \tag{1.1}$$

and the 1D compressible Euler equations of gas dynamics:

$$w_t + f(w)_x = 0, \qquad w(x,0) = w_0(x), \tag{1.2}$$

where

$$w = \begin{pmatrix} \rho \\ m \\ E \end{pmatrix}, \quad f(w) = \begin{pmatrix} w_2 \\ w_2^2/w_1 + p \\ w_2(w_3+p)/w_1 \end{pmatrix}. \tag{1.3}$$

Periodic boundary conditions are imposed, with (x,t) ranging over $[a,b] \times [0,T]$, where T is the final time. The physical variables—density ρ, velocity u, momentum m, total energy E, pressure p, and internal energy e—are related via $m = \rho u$, $E = \frac{1}{2}\rho u^2 + \rho e$, and $p = (\gamma - 1)\rho e$, where $\gamma > 1$ is the adiabatic index ($\gamma = 1.4$ for air). Here, $c = \sqrt{\gamma p/\rho}$ is the speed of sound, and $u - c$, u, and $u + c$ are the eigenvalues of the Jacobian matrix $f'(w)$.

The exact solutions to these equations satisfy important physical principles, including conservation, the maximum principle (in the scalar case (1.1)), and positivity of density and pressure (in the Euler system (1.2)). Preserving these properties at the discrete level is essential for ensuring the physical reliability of numerical simulations. However,

Received: 12 September 2025; Accepted: 01 July 2026.
∗ Corresponding author. Email: farzi@sut.ac.ir.

conventional high-order schemes may generate nonphysical artifacts such as overshoots, undershoots, or negative densities and pressures—particularly near discontinuities—due to numerical oscillations. To address these challenges, several numerical schemes have been proposed, including Runge-Kutta discontinuous Galerkin (DG) methods [4], finite volume and finite difference WENO methods [6, 9], and spectral volume (SV) methods [23]. While these methods reduce oscillations, they can still fail to satisfy the discrete maximum principle (DMP) or the positivity-preserving (PP) condition. Therefore, additional modifications are required to enforce these properties in high-order schemes.

For the scalar case, the entropy solution satisfies the maximum principle. If $M = \max_x u_0(x)$ and $m = \min_x u_0(x)$, then

$$u(x,t) \in [m, M], \quad \forall x, t. \tag{1.4}$$

A corresponding numerical scheme should enforce this condition discretely:

$$\bar{u}_j^n \in [m, M], \quad \forall n, j, \tag{1.5}$$

where $\bar{u}_j^n$ denotes the cell average at time level n. Moreover, if the initial data is nonnegative, the solution remains nonnegative:

$$u_0(x) \geq 0 \Longrightarrow u(x,t) \geq 0, \quad \forall t \geq 0, \tag{1.6}$$

and the proposed scheme must preserve this property:

$$\bar{u}_j^n \geq 0, \quad \forall n, j. \tag{1.7}$$

In practice, standard monotone schemes satisfying the maximum principle are at most second-order accurate [10]. Thus, high-order methods require additional strategies to ensure MPP properties. Two major approaches have been proposed. The first approach involves parametrized MPP flux limiters introduced by Xu [28], designed to adjust high-order fluxes so they satisfy the DMP. In [25], this limiter is enforced only during the last stage of Runge-Kutta WENO schemes, allowing larger time steps while preserving high-order accuracy. Christlieb et al. [2] extended this approach to high-order ENO/WENO schemes. Xiong et al. applied the limiter to DG schemes for convection-diffusion equations [26], while Yang [29] and Liang [12] further generalized it to other frameworks including finite volume methods. Farzi [15] adapted the limiter for SV methods with TVD Runge-Kutta integration. The second approach, proposed by Zhang and Shu [30], modifies the reconstruction polynomial itself. Unlike flux limiters, this method enforces the DMP by scaling the polynomial. It was inspired by a linear rescaling technique developed by Liu and Osher [14], and has been applied to DG and WENO discretizations coupled with strong stability preserving time integration. Although effective, this approach may require more restrictive CFL conditions to maintain both accuracy and the MPP property [30]. Extensions include DG schemes on triangular meshes [31], convection-diffusion equations [32], and compact WENO schemes [8]. Applications have also been reported for traffic flow on networks [19] and scalar conservation laws using MPP finite element techniques [7]. Additional implementations include DG schemes for transport equations [27] and central DG schemes for hyperbolic conservation laws [13].

For the compressible Euler system (1.2), although the maximum principle does not generally apply, physical variables like density and pressure must remain positive. Several first-order schemes ensure positivity preservation [16], but high-order schemes may produce unphysical negative values, particularly under strong shocks. The framework by Zhang and Shu [33] ensures positivity while maintaining high-order accuracy, and has been extended to DG [17, 34] and WENO schemes [2, 3, 18].

In this paper, we extend the MPP/PP limiting framework of Zhang and Shu [30] to spectral volume schemes for both scalar equations and the compressible Euler system. The SV scheme, introduced by Wang et al. [23], is a high-order conservative Godunov-type method. Each SV is subdivided into control volumes (CVs), and polynomial reconstruction is performed using only local CV data. Unlike high-order finite volume methods (e.g., WENO [6] or k-exact methods [1]), which require wide stencils, the SV method relies solely on intra-cell information, reducing memory usage and computational cost. Moreover, polynomial evaluations are performed at Legendre-Gauss-Lobatto points, improving accuracy and stability.

The organization of the rest of this paper is as follows; In section 2, the SV method for one-dimensional scalar conservation laws is introduced. Section 3 presents the MPP limiter for the SV method. In section 4, we extend

the approach to enforce positivity for the compressible Euler equations. Numerical results validating the proposed MPP/PP schemes are provided in section 5. Concluding remarks are presented in section 6.

2. SV Methods for Hyperbolic Conservation Laws

Let us consider the one-dimensional hyperbolic conservation law (1.1), and partition the domain $D = [a, b]$ as follows:

$$D = \bigcup_{i=1}^{N} S_i, \quad S_i = [x_{i-\frac{1}{2}}, x_{i+\frac{1}{2}}], \tag{2.1}$$

where $\{x_{i+\frac{1}{2}}\}_{i=0}^{N}$ denotes a set of $N+1$ partitioning points in $[a, b]$, which define N non-overlapping cells S_i, $i = 1, \ldots, N$, referred to as *spectral volumes* (SVs).

Let $h_i = x_{i+\frac{1}{2}} - x_{i-\frac{1}{2}}$ and define $h = \max_{1\le i\le N} h_i$. For a given approximation order k, each SV S_i is further subdivided into k subcells using the points $\{x_{i,j+\frac{1}{2}}\}_{j=0}^{k}$, where $x_{i,\frac{1}{2}} = x_{i-\frac{1}{2}}$ and $x_{i,k+\frac{1}{2}} = x_{i+\frac{1}{2}}$. These subcells will be addressed as *control volumes* (CVs) and denoted by $C_{i,j}$:

$$C_{i,j} = (x_{i,j-\frac{1}{2}}, x_{i,j+\frac{1}{2}}), \quad j = 1, \ldots, k. \tag{2.2}$$

The cell average of the state variable u at time t over the control volume $C_{i,j}$ is defined as:

$$\overline{u}_{i,j}(t) = \frac{1}{h_{i,j}} \int_{x_{i,j-\frac{1}{2}}}^{x_{i,j+\frac{1}{2}}} u(x,t)\, dx, \quad j = 1, \ldots, k, \quad i = 1, \ldots, N, \tag{2.3}$$

where $h_{i,j} = x_{i,j+\frac{1}{2}} - x_{i,j-\frac{1}{2}}$ is the width of $C_{i,j}$.

Using the k available CV-averages in S_i, we reconstruct a kth-order polynomial $p_i(x)$ approximating $u(x)$ within the SV S_i:

$$p_i(x) = u(x) + \mathcal{O}(h^k), \quad x \in S_i, \quad i = 1, \ldots, N. \tag{2.4}$$

The reconstruction polynomial p_i must satisfy the following moment-matching condition:

$$\frac{1}{h_{i,j}} \int_{x_{i,j-\frac{1}{2}}}^{x_{i,j+\frac{1}{2}}} p_i(x)\, dx = \overline{u}_{i,j}(t), \quad j = 1, \ldots, k. \tag{2.5}$$

This constraint ensures a unique reconstruction. The main purpose of $p_i(x)$ is to approximate the state variable at CV interfaces:

$$u_{i,j+\frac{1}{2}} \equiv p_i(x_{i,j+\frac{1}{2}}) = u(x_{i,j+\frac{1}{2}}) + \mathcal{O}(h^k), \quad j = 0, \ldots, k, \quad i = 1, \ldots, N. \tag{2.6}$$

From (2.5), it follows that the coefficients of p_i depend linearly on the CV averages $\overline{u}_{i,j}$, the mesh sizes $h_{i,j}$, and the approximation order k. Hence, the interface values $u_{i,j+\frac{1}{2}}$ can be written as:

$$u_{i,j+\frac{1}{2}} = \sum_{l=1}^{k} c_{jl}\, \overline{u}_{i,l}, \quad j = 0, \ldots, k, \tag{2.7}$$

where the coefficients c_{jl} depend on k and the local mesh configuration.

To compute c_{jl}, we follow the reconstruction strategy introduced by Shu in [21], assuming the form:

$$p_i(x) = \sum_{l=1}^{k} \phi_l(x)\, \overline{u}_{i,l}. \tag{2.8}$$

Following [21, 23], this approach utilizes the primitive function of $u(x)$ in S_i, leading to the coefficients:

$$c_{jl} = \phi_l(x_{i,j+\frac{1}{2}}) = h_{i,l} \sum_{r=l}^{k} \frac{1}{\varpi'(x_{i,r+\frac{1}{2}})} \sum_{\substack{m=0 \\ m\neq r}}^{k} \prod_{\substack{q=0 \\ q\neq m,r}}^{k} (x_{i,j+\frac{1}{2}} - x_{i,q+\frac{1}{2}}), \tag{2.9}$$

where

$$\varpi(x) = (x - x_{i,\frac{1}{2}})(x - x_{i,\frac{3}{2}}) \dots (x - x_{i,k+\frac{1}{2}}). \tag{2.10}$$

If the control volumes are of uniform size, then the coefficients simplify to:

$$c_{jl} = \sum_{r=l}^{k} \frac{1}{\prod_{\substack{q=0 \\ q\neq r}}^{k} (r-q)} \sum_{\substack{m=0 \\ m\neq r}}^{k} \prod_{\substack{q=0 \\ q\neq m,r}}^{k} (j-q). \tag{2.11}$$

By performing the integration of (1.1) over a generic control volume $C_{i,j}$ and assuming CVs are treated independently, we obtain the semi-discrete formulation:

$$\frac{d\overline{u}_{i,j}}{dt} h_{i,j} + (F_{i,j+\frac{1}{2}} - F_{i,j-\frac{1}{2}}) = 0, \tag{2.12}$$

where $F_{i,j+\frac{1}{2}}$ denotes the numerical flux at $x_{i,j+\frac{1}{2}}$.

Since the reconstructed field is discontinuous at the boundaries of each S_i, fluxes at these boundaries must be computed using a Riemann solver:

$$F_{i,\frac{1}{2}} = F_{\text{Riemann}}(u_{i-1,k+\frac{1}{2}}, u_{i,\frac{1}{2}}), \tag{2.13}$$

$$F_{i,k+\frac{1}{2}} = F_{\text{Riemann}}(u_{i,k+\frac{1}{2}}, u_{i+1,\frac{1}{2}}). \tag{2.14}$$

Within each SV, where the reconstruction is continuous, analytical fluxes can be directly evaluated at interior CV boundaries:

$$F_{i,j+\frac{1}{2}} = f(u_{i,j+\frac{1}{2}}), \quad j = 1, \dots, k-1. \tag{2.15}$$

Common numerical flux functions include:

1. **Lax-Friedrichs flux**:

$$F_{LF}(u_l, u_r) = \frac{1}{2}\left[f(u_l) + f(u_r) - \alpha(u_r - u_l)\right], \quad \alpha = \max_u |f'(u)|. \tag{2.16}$$

   The flux is termed *global* if α is computed over the entire domain of u, and *local* if restricted to the interval $[u_l, u_r]$.

2. **Roe flux with entropy fix**:

$$F_R(u_l, u_r) = \begin{cases} f(u_l), & \text{if } f'(u) \geq 0 \text{ for } u \in [\min(u_l, u_r), \max(u_l, u_r)], \\ f(u_r), & \text{if } f'(u) \leq 0 \text{ for } u \in [\min(u_l, u_r), \max(u_l, u_r)], \\ F_{LF}(u_l, u_r), & \text{Otherwise.} \end{cases} \tag{2.17}$$

For time integration of (2.12), we employ the total variation diminishing (TVD) Runge-Kutta methods [20]. The system is rewritten as:

$$\frac{d\overline{u}}{dt} = L(\overline{u}), \tag{2.18}$$

where

$$\overline{u} = [\overline{u}_{i,j}]_{j=1}^{k}, \quad L(\overline{u}) = [L_{i,j}(\overline{u})]_{j=1}^{k}, \tag{2.19}$$

$$L_{i,j} = -\frac{1}{h_{i,j}} \left(F_{i,j+\frac{1}{2}} - F_{i,j-\frac{1}{2}}\right). \tag{2.20}$$

Let $\overline{v}^{(0)} = \overline{u}^n$, and set $\overline{u}^{n+1} = \overline{v}^{(3)}$. The third-order TVD Runge-Kutta scheme is given by:

$$\begin{aligned}
\overline{v}^{(1)} &= \overline{v}^{(0)} + \Delta t\, L(\overline{v}^{(0)}),\\
\overline{v}^{(2)} &= \frac{3}{4}\overline{v}^{(0)} + \frac{1}{4}\left[\overline{v}^{(1)} + \Delta t\, L(\overline{v}^{(1)})\right],\\
\overline{v}^{(3)} &= \frac{1}{3}\overline{v}^{(0)} + \frac{2}{3}\left[\overline{v}^{(2)} + \Delta t\, L(\overline{v}^{(2)})\right].
\end{aligned} \tag{2.21}$$

We conclude this section by discussing the choice of partitioning points for constructing the control volumes. The SV method uses only the local information within each SV, avoiding wide stencils and enhancing computational efficiency. The choice of partitioning points, whether uniform or non-uniform, significantly affects the stability and smoothness of high-order reconstructions.

For $k > 3$, uniform CV partitioning can introduce strong oscillations near SV boundaries. To mitigate this, clustering nodes such as Gauss-Lobatto points are employed:

$$x_{i,j+\frac{1}{2}} = -\cos\left(\frac{j\pi}{k}\right), \quad j = 0, \ldots, k, \tag{2.22}$$

defined on the standard interval $[-1, 1]$. These points help reduce endpoint oscillations.

Alternatively, a hyperbolic tangent clustering can be used:

$$x_{i,j+\frac{1}{2}} = \frac{\tanh\left(\frac{2\mu j}{k} - \mu\right)}{\tanh(\mu)}, \quad j = 0, \ldots, k, \tag{2.23}$$

where μ controls the grid density near the SV boundaries. For a comprehensive discussion of clustering strategies in spectral volume methods, see [23].

3. Maximum-Principle-Preserving SV Scheme for Scalar Equations

This section uses the limiter from [30] to regulate the maximum/minimum of the reconstruction polynomial derived from the SV method for scalar hyperbolic conservation laws in one dimension, as given in equation (1.1). We first discuss the Euler forward temporal discretization, and subsequently consider higher-order temporal discretization methods.

The discretized form of (2.18) using the Euler forward method is expressed as:

$$\overline{u}_{i,j}^{n+1} = \overline{u}_{i,j}^{n} - \lambda_{i,j}\left[F_{i,j+\frac{1}{2}}(\overline{u}) - F_{i,j-\frac{1}{2}}(\overline{u})\right], \tag{3.1}$$

where $\lambda_{i,j} = \frac{\Delta t}{h_{i,j}}$. For implementation of (3.1), it is crucial to compute the numerical flux function $F(.,.)$ at both ends of each SV S_i, which typically requires an exact or approximate Riemann solver. We will utilize a monotone flux, as specified in [5], where the monotone flux $F(.,.)$ results in a first-order monotone scheme that keeps the strict maximum principle property. We have the following lemma to prove this result for the Lax-Friedrichs flux (2.16), where $F_{i,j+\frac{1}{2}}(\overline{u}) = F_{LF}(\overline{u}_{i,j}^{n}, \overline{u}_{i,j+1}^{n})$.

Lemma 3.1. *Consider the first-order Lax–Friedrichs scheme under the CFL condition $\lambda a \le 1$, where $\lambda = \max_{i,j} \lambda_{i,j}$ and $a = \max|f'(u)|$. If $\overline{u}_{i,j}^{n} \in [m, M]$ for all i, j, then $\overline{u}_{i,j}^{n+1} \in [m, M]$ for all i, j.*

Proof. Let us consider the first order scheme with the Lax–Friedrichs flux:

$$\overline{u}_{i,j}^{n+1} = \overline{u}_{i,j}^{n} - \lambda_{i,j}[F_{LF}(\overline{u}_{i,j}^{n}, \overline{u}_{i,j+1}^{n}) - F_{LF}(\overline{u}_{i,j-1}^{n}, \overline{u}_{i,j}^{n})]. \tag{3.2}$$

For simplicity, let

$$u = \overline{u}_{i,j}^{n}, \quad u_+ = \overline{u}_{i,j+1}^{n}, \quad u_- = \overline{u}_{i,j-1}^{n}, \quad \lambda = \lambda_{i,j}.$$

Then the scheme becomes

$$\overline{u}^{n+1} = u - \tfrac{\lambda}{2}\big(f(u_+) - f(u_-)\big) + \tfrac{\lambda a}{2}(u_+ - 2u + u_-).$$

By the mean value theorem, there exists ξ between u_- and u_+ such that

$$f(u_+) - f(u_-) = f'(\xi)(u_+ - u_-).$$

Substituting this gives

$$\overline{u}^{n+1} = u + \tfrac{\lambda}{2}\Big((a - f'(\xi))u_+ - 2a\,u + (a + f'(\xi))u_-\Big).$$

This can be written as a convex combination:

$$\overline{u}^{n+1} = \alpha u_- + \beta u + \gamma u_+,$$

where

$$\alpha = \tfrac{\lambda}{2}(a + f'(\xi)), \quad \gamma = \tfrac{\lambda}{2}(a - f'(\xi)), \quad \beta = 1 - \lambda a.$$

Clearly, $\alpha + \beta + \gamma = 1$. Moreover, since $|f'(\xi)| \le a$, we have $a \pm f'(\xi) \ge 0$, hence $\alpha \ge 0$ and $\gamma \ge 0$. The CFL condition $\lambda a \le 1$ ensures $\beta \ge 0$. Therefore, all coefficients α, β, γ are nonnegative and sum to 1.

Thus $\overline{u}^{n+1}$ is a convex combination of u_-, u, u_+. If all three values lie in the interval $[m, M]$, then so does their convex combination. Since this holds for every cell, the maximum principle is preserved:

$$m \le \overline{u}_{i,j}^{n+1} \le M, \quad \forall i, j.$$

□ □

We proceed with high order reconstruction with the polynomial p_i in the spectral volume S_i. We need to limit the nodal values $u^+_{i,j-1/2}$ and $u^-_{i,j+1/2}$ in some way so that $\overline{u}_{i,j}^{n+1} \in [m, M]$ reduces whenever $\overline{u}_{i,j}^{n} \in [m, M]$. Noting that the N-point Legendre–Gauss–Lobatto quadrature rule integrates polynomials of degree up to $2N-3$ exactly over the interval $C_{i,j} = [x_{i,j-1/2}, x_{i,j+1/2}]$, its application yields a sufficient condition to ensure that $\overline{u}_{i,j}^{n+1} \in [m, M]$ holds for the numerical scheme (3.1).

Denote LGL nodes as follows

$$B_{i,j} = \left\{\hat{x}^l_{i,j},\, l = 1, \dots, N\right\}, \tag{3.3}$$

where, $x_{i,j-1/2} = \hat{x}^1_{i,j}, \hat{x}^N_{i,j} = x_{i,j+1/2}$, and let $\omega = \{\hat{\omega}^\alpha, \alpha = 1, \dots, N\}$ be the quadrature weights for the interval $[-\frac{1}{2}, \frac{1}{2}]$ such that $\sum_{\alpha=1}^{N} \hat{\omega}^\alpha = 1$. Define $\hat{\nu}_{i,\alpha} = p_i(\hat{x}^\alpha_{i,j})$ and select N so that be the smallest integer satisfying $2N - 3 \ge k$, therefore

$$\overline{u}^n_{i,j} = \frac{1}{h_{i,j}} \int_{C_{i,j}} p_i(x)dx = \sum_{\alpha=1}^{N} \hat{\omega}^\alpha \hat{\nu}_{i,\alpha}. \tag{3.4}$$

In the following theorem, for convenience, in the cell $C_{i,j}$, if $j = 1$ we denote $\hat{\nu}_{i,0} = u_{i-1,k+\frac{1}{2}}$, and if $j = k$ we denote $\hat{\nu}_{i,N+1} = u_{i+1,\frac{1}{2}}$ and otherwise we denote $\hat{\nu}_{i,0} = u_{i,j-\frac{1}{2}}$ and $\hat{\nu}_{i,N+1} = u_{i,j+\frac{1}{2}}$.

Theorem 3.2. *Consider a spectral volume method with the Lax–Friedrichs flux (2.16) applied at the two ends of each S_i, and let $p_i(x)$ be the reconstruction polynomial of degree k on S_i. If the point values $\hat{\nu}_{i,\alpha}$ $(\alpha = 0, \dots, N+1)$ and the CV averages $\overline{u}^n_{i,j}$ all lie in the interval $[m, M]$, then $\overline{u}^{n+1}_{i,j} \in [m, M]$ under the CFL condition*

$$\lambda a \le \min_\alpha \hat{\omega}_\alpha, \tag{3.5}$$

where $\lambda = \max_{i,j} \lambda_{i,j}$ and $a = \max |f'(u)|$.

Proof. The proof proceeds by expressing each cell-average update as a convex combination of one-step Lax–Friedrichs-type updates and then invoking the scalar maximum-principle preservation of the first-order Lax–Friedrichs scheme.

Fix an SV index i and a CV index j. By the spectral-volume reconstruction and the quadrature relation (3.4) we may write the cell average $\overline{u}^n_{i,j}$ (and similarly the flux difference appearing in the update) as a weighted sum over the

reconstruction nodes $\{\hat{\nu}_{i,\alpha}\}$ with positive weights $\{\hat{\omega}^\alpha\}$ satisfying $\sum_\alpha \hat{\omega}^\alpha = 1$. In particular, for the flux difference that enters the update formula (3.1) one has the identity

$$F(u_{i,j+\frac{1}{2}}) - F_{\mathrm{LF}}(\text{left data}, \text{right data}) = \sum_{\alpha=1}^{N} \left[F_{\mathrm{LF}}(\hat{\nu}_{i,\alpha}, \hat{\nu}_{i,\alpha+1}) - F_{\mathrm{LF}}(\hat{\nu}_{i,\alpha-1}, \hat{\nu}_{i,\alpha})\right],$$

so that the update for $\overline{u}_{i,j}$ can be rearranged as

$$\overline{u}_{i,j}^{n+1} = \sum_{\alpha=1}^{N} \hat{\omega}^\alpha \Big(\hat{\nu}_{i,\alpha} - \frac{\lambda_{i,j}}{\hat{\omega}^\alpha}\left[F_{\mathrm{LF}}(\hat{\nu}_{i,\alpha}, \hat{\nu}_{i,\alpha+1}) - F_{\mathrm{LF}}(\hat{\nu}_{i,\alpha-1}, \hat{\nu}_{i,\alpha})\right]\Big). \tag{3.6}$$

Define, for each α,

$$G_{i,j}^\alpha := \hat{\nu}_{i,\alpha} - \frac{\lambda_{i,j}}{\hat{\omega}^\alpha}\left[F_{\mathrm{LF}}(\hat{\nu}_{i,\alpha}, \hat{\nu}_{i,\alpha+1}) - F_{\mathrm{LF}}(\hat{\nu}_{i,\alpha-1}, \hat{\nu}_{i,\alpha})\right].$$

Then (3.6) reads $\overline{u}_{i,j}^{n+1} = \sum_\alpha \hat{\omega}^\alpha G_{i,j}^\alpha$.

We now show that each $G_{i,j}^\alpha \in [m, M]$. Observe that $G_{i,j}^\alpha$ has exactly the form of a single-step Lax–Friedrichs update applied to the triple $(\hat{\nu}_{i,\alpha-1}, \hat{\nu}_{i,\alpha}, \hat{\nu}_{i,\alpha+1})$ but with a local time-step coefficient $\widetilde{\lambda}^\alpha := \dfrac{\lambda_{i,j}}{\hat{\omega}^\alpha}$. Indeed, using the LF flux $F_{\mathrm{LF}}(x, y) = \frac{1}{2}\big(f(x) + f(y) - a(y - x)\big)$ one rewrites

$$G_{i,j}^\alpha = \hat{\nu}_{i,\alpha} - \widetilde{\lambda}^\alpha\big(F_{\mathrm{LF}}(\hat{\nu}_{i,\alpha}, \hat{\nu}_{i,\alpha+1}) - F_{\mathrm{LF}}(\hat{\nu}_{i,\alpha-1}, \hat{\nu}_{i,\alpha})\big),$$

which is precisely the Lax–Friedrichs one-step formula (compare with Lemma for the scalar case).

By the assumption $\hat{\nu}_{i,\alpha-1}, \hat{\nu}_{i,\alpha}, \hat{\nu}_{i,\alpha+1} \in [m, M]$ and by the scalar maximum-principle preservation of the first-order Lax–Friedrichs update (cf. the Lemma 3.1), it suffices to ensure the CFL condition for this local step:

$$\widetilde{\lambda}^\alpha\, a \;=\; \frac{\lambda_{i,j}}{\hat{\omega}^\alpha}\, a \;\le\; 1.$$

Thus, if for the given cell we require

$$\lambda_{i,j} a \le \min_\alpha \hat{\omega}^\alpha,$$

then every $\widetilde{\lambda}^\alpha a \le 1$ and therefore $G_{i,j}^\alpha \in [m, M]$ for all α.

Finally, since $\{\hat{\omega}^\alpha\}$ are nonnegative weights summing to one, the representation $\overline{u}_{i,j}^{n+1} = \sum_\alpha \hat{\omega}^\alpha G_{i,j}^\alpha$ is a convex combination of values in $[m, M]$, and hence $\overline{u}_{i,j}^{n+1} \in [m, M]$. As this argument holds for every CV index j and SV index i, the theorem follows. □ □

Following this theorem, the reconstruction polynomial needs to be adjusted so that its values $p_i(x)$ fall within the range of m to M for all x in S_i. The primary challenge lies in maintaining cell averages through a limiting process. Limiting the reconstruction polynomial is not straightforward as in the case of TVD/TVB limiters, because it directly modifies the cell boundary values, however, the focus of MPP limiter is on modifying the reconstruction polynomial and it requires the constraint of maintaining the prescribed cell averages. In this regard, limiting based on the spectral volume is not a trivial task, and proceeding with respect to the control volume, the reconstruction polynomial p_i must be restricted to the control volume $C_{i,j}$ prior to enforcement of the the maximum principle property. The reconstruction within the spectral volume S_i can be discontinuous across neighboring cells.

For all j, assume $\overline{u}_{i,j}^n \in [m, M]$, we introduce the modified polynomial $\tilde{p}_{i,j}(x)$ as follows

$$\tilde{p}_{i,j}(x) = \theta(p_i(x) - \overline{u}_{i,j}^n) + \overline{u}_{i,j}^n, \quad \theta = \min\left\{\left|\frac{M - \overline{u}_{i,j}^n}{M_{i,j} - \overline{u}_{i,j}^n}\right|, \left|\frac{m - \overline{u}_{i,j}^n}{m_{i,j} - \overline{u}_{i,j}^n}\right|, 1\right\}, \tag{3.7}$$

with

$$M_{i,j} = \max_{x \in C_{i,j}} p_i(x), \; m_{i,j} = \min_{x \in C_{i,j}} p_i(x). \tag{3.8}$$

Let $\tilde{u}^{+}_{i,j-1/2} = \tilde{p}_{i,j}(x_{i,j-1/2})$ and $\tilde{u}^{-}_{i,j+1/2} = \tilde{p}_{i,j}(x_{i,j+1/2})$, in this case we obtain an improved version of (3.1) as following:

$$\overline{u}^{n+1}_{i,j} = \overline{u}^{n}_{i,j} - \lambda_{i,j}[F(\tilde{u}^{-}_{i,j+1/2}, \tilde{u}^{+}_{i,j+1/2}) - F(\tilde{u}^{-}_{i,j-1/2}, \tilde{u}^{+}_{i,j-1/2})]. \tag{3.9}$$

The uniform high order of accuracy of underlying limiter is denoted in the following lemma.

Lemma 3.3. *Let $\overline{u}^{n}_{i,j} \in [m, M]$. Then the definitions (3.7) and (3.8) yield a $(k+1)$th order accurate limiter.*

Proof. We need to show that $\tilde{p}_{i,j}(x) - p_i(x) = O(h^{k+1})$ for any $x \in C_{i,j}$, where $h = \max_{i,j} h_{i,j}$. We only prove the case when $p_i(x)$ is not constant and

$$\theta = \frac{M - \overline{u}^{n}_{i,j}}{M_{i,j} - \overline{u}^{n}_{i,j}},$$

the other cases being analogous. Since $\overline{u}^{n}_{i,j} \le M$ and $\overline{u}^{n}_{i,j} \le M_{i,j}$, we obtain

$$\begin{aligned}
\tilde{p}_{i,j}(x) - p_i(x) &= \theta\big(p_i(x) - \overline{u}^{n}_{i,j}\big) + \overline{u}^{n}_{i,j} - p_i(x) \\
&= (\theta - 1)\big(p_i(x) - \overline{u}^{n}_{i,j}\big) \\
&= \frac{M - M_{i,j}}{M_{i,j} - \overline{u}^{n}_{i,j}}\big(p_i(x) - \overline{u}^{n}_{i,j}\big).
\end{aligned}$$

From the definition of θ in (3.7), we have $\theta < 1$, which corresponds to an overshoot, i.e. $M < M_{i,j}$. Since $p_i(x)$ is a degree-k polynomial reconstruction with error $O(h^{k+1})$, it follows that

$$M_{i,j} - M = O(h^{k+1}).$$

Thus, it remains to show that

$$\left|\frac{p_i(x) - \overline{u}^{n}_{i,j}}{M_{i,j} - \overline{u}^{n}_{i,j}}\right| \le C_k,$$

for some constant C_k depending only on k. To this end, write

$$p_i(x) = a_0 + a_1\Big(\tfrac{x - x_{i,j}}{h_{i,j}}\Big) + \cdots + a_k\Big(\tfrac{x - x_{i,j}}{h_{i,j}}\Big)^k,$$

and consider the rescaled polynomial

$$p(x) = a_0 + a_1 x + \cdots + a_k x^k, \qquad x \in I = [-\tfrac{1}{2}, \tfrac{1}{2}].$$

The cell average of $p(x)$ on I is $\overline{p} = \overline{u}^{n}_{i,j}$, and $\max_{x\in I} p(x) = M_{i,j}$. Therefore,

$$\max_{x\in C_{i,j}} \left|\frac{p_i(x) - \overline{u}^{n}_{i,j}}{M_{i,j} - \overline{u}^{n}_{i,j}}\right| = \max_{x\in I} \left|\frac{p(x) - \overline{p}}{\max_{y\in I} p(y) - \overline{p}}\right|.$$

The numerator and denominator define equivalent norms on the finite-dimensional space P^k of polynomials of degree at most k. Hence, the quotient is uniformly bounded by a constant C_k depending only on k. Combining this with the factor $M - M_{i,j} = O(h^{k+1})$ proves the claim. □

Since it is sufficient to control the values at the quadrature points, Equation (3.8) can be replaced by:

$$M_{i,j} = \max_{x\in B_{i,j}} p_i(x), \; m_{i,j} = \min_{x\in B_{i,j}} p_i(x), \tag{3.10}$$

and enforcing limiter (3.7) with (3.10) is sufficient to ensure this condition is met

$$\tilde{p}_{i,j}(x) \in [m, M]. \tag{3.11}$$

By replacing (3.8) with (3.10), the accuracy of the scheme is preserved, and its conservativeness is maintained, since the modification does not alter the cell average of the polynomial.

Theorem 3.4. *Assume that $p_i(x)$ is an SV-reconstruction polynomial of degree k, and let m and M be defined in (1.4). If the scheme (3.1) is $(k+1)$th-order accurate for smooth solutions and satisfies $\overline{u}_{i,j}^n \in [m, M]$, then the revised scheme, consisting of (3.7), (3.10), and (3.9), also achieves $(k+1)$th-order accuracy and preserves the maximum principle*

$$\overline{u}_{i,j}^{n+1} \in [m, M],$$

under the CFL condition specified in (3.5).

Proof. Define $\tilde{\nu}_{i,j,\alpha} = \tilde{p}_{i,j}(\hat{x}_{i,j}^{\alpha})$ for $\alpha = 1, \ldots, N$. For the boundary cases, set

$$\tilde{\nu}_{i1,0} = \tilde{p}_{i-1,k}(\hat{x}_{i,1}^{1}), \qquad \tilde{\nu}_{i1,N+1} = \tilde{p}_{i,2}(\hat{x}_{i,1}^{N}),$$

when $j = 1$, and

$$\tilde{\nu}_{ik,0} = \tilde{p}_{i,k-1}(\hat{x}_{i,k}^{1}), \qquad \tilde{\nu}_{ik,N+1} = \tilde{p}_{i+1,1}(\hat{x}_{i,k}^{N}),$$

when $j = k$. For the interior indices $j \neq 1, k$, define

$$\tilde{\nu}_{i,j,0} = \tilde{p}_{i,j-1}(\hat{x}_{i,j}^{1}), \qquad \tilde{\nu}_{i,j,N+1} = \tilde{p}_{i,j+1}(\hat{x}_{i,j}^{N}).$$

With these definitions, the limiter given in (3.7) and (3.10) guarantees that all revised values $\tilde{\nu}_{i,j,\alpha}$ lie within $[m, M]$. By Theorem 3.2, it then follows that the maximum principle is preserved, i.e.

$$\overline{u}_{i,j}^{n+1} \in [m, M].$$

This completes the proof. □ □

Remark 3.5. The high order SSP time discretization, being a convex combination of Euler forward, will indeed satisfy the MPP property.

4. Positivity preserving limiters for Euler systems

This section extends the positivity preserving limiters developed in [31] to kth order accurate spectral finite volume scheme for solving compressible Euler equations of gas dynamics.

4.1. SV scheme for Euler systems.

The SV scheme for (1.2) is

$$\frac{d\overline{w}_{i,j}}{dt} h_{i,j} + (F_{i,j+1/2}(\bar{w}) - F_{i,j-1/2}(\bar{w})) = 0, \tag{4.1}$$

where the numerical flux $F_{i,j+1/2}$ is a vector function of mass, momentum and total energy at the CV boundary namely $x_{i,j+1/2}$ and is defined by

$$F_{i,1/2} = F_{\text{Riemann}}(w_{i-1,k+1/2}, w_{i,1/2}), \tag{4.2}$$

similarly

$$F_{i,k+1/2} = F_{\text{Riemann}}(w_{i,k+1/2}, w_{i+1,1/2}). \tag{4.3}$$

Due to the continuity of the reconstructed field at internal control volume interfaces within a spectral volume, the numerical flux coincides with the exact flux function.

$$F_{i,j+1/2} = F(w_{i,j+1/2}), \;\; j = 1, \ldots, k-1. \tag{4.4}$$

Note that $w_{i,j+1/2}$, $i = 1, \ldots, N, j = 0, \ldots, k$ are the high order approximations of the point values $w(x_{i,j+1/2}, t^n), i = 1, \ldots, N, j = 0, \ldots, k$. These values are obtained from polynomial vectors $\mathbf{q}_i(x) = (\rho_i(x), m_i(x), E_i(x))^T$ with degree k, where $k \geq 1$, defined on S_i, that are reconstructed from a high order SV approximation, which was discussed in the section 2.

4.2. **Positivity preserving limiters.** The primary aim of this subsection is to design a conservative, positivity-preserving SV scheme with high-order accuracy for the numerical solution of the compressible Euler equations governing gas dynamics. We first employ the first-order Euler forward method for time discretization, providing a foundation for the development of more advanced higher-order techniques, which will be addressed subsequently. The Euler forward temporal discretization of Equation (4.1) is formulated as follows:

$$\overline{w}_{i,j}^{n+1} = \overline{w}_{i,j}^{n} - \lambda_{i,j}[F_{i,j+\frac{1}{2}}(\overline{w}) - F_{i,j-\frac{1}{2}}(\overline{w})], \tag{4.5}$$

where $\lambda_{i,j} = \frac{\Delta t}{h_{i,j}}$.

Let $p(w) = (\gamma - 1)\left(E - \frac{m^2}{2\rho}\right)$ denote the pressure function. It can be shown that the eigenvalues of the Hessian matrix $\frac{\partial^2}{\partial w^2} p$ are nonpositive if and only if $\rho > 0$. Therefore, p is a concave function of $w = (\rho, m, E)^T$ whenever $\rho \geq 0$, and it satisfies Jensen's inequality. Specifically, for $w_1 = (\rho_1, m_1, E_1)^T$ and $w_2 = (\rho_2, m_2, E_2)^T$, and for any $0 \leq s \leq 1$, we have

$$p(sw_1 + (1-s)w_2) \geq sp(w_1) + (1-s)p(w_2), \text{ if } \rho_1 \geq 0, \ \rho_2 \geq 0. \tag{4.6}$$

The set of admissible states is defined as

$$G = \left\{ w \middle| \rho > 0, \ p > 0 \right\}, \tag{4.7}$$

then G is a convex set.

We aim to introduce a positivity preserving limiter for the SV scheme, such that the cell averages of the numerical solution at each grid point $C_{i,j}$ remain within the set G at every time step t_n. This is achieved by employing the N-point Legendre Gauss-Lobatto quadrature rule on each $C_{i,j}$, which provides exact results for the integration of polynomials of degree up to $2N-3$. We determine these points as (3.3) on each $C_{i,j}$ and let $\omega = \{\hat{\omega}^\alpha, \alpha = 1, \ldots, N\}$ be the quadrature weights for the interval $[-\frac{1}{2}, \frac{1}{2}]$ such that $\sum_{\alpha=1}^{N} \hat{\omega}^\alpha = 1$.

Theorem 4.1. *Let $\bar{w}_{i,j}^{n+1}$ be an approximation produced by a kth order reconstruction in the scheme (4.5), a sufficient condition for $\bar{w}_{i,j}^{n+1} \in G$ is*

$$\boldsymbol{q}_i(\hat{x}_{i,j}^{\alpha}) \in G, \ \forall j, \alpha, \tag{4.8}$$

under the CFL condition

$$\lambda \|(|u| + c)\|_\infty \leq \hat{\omega}^1 \alpha_0, \tag{4.9}$$

where $\lambda = \max_{i,j} \lambda_{i,j}$ and α_0 is a constant depending on the specific scheme.

The proof is mainly simillar to the proof of positivity in [31] for finite volume methods and we omit it.

Following this theorem, it is necessary to modify $\mathbf{q}_i(x)$ on each $C_{i,j}$ so that $\mathbf{q}_i(x) \in G$ for all $x \in B_{i,j}$. Modifing $\mathbf{q}_i(x)$ on each $C_{i,j}$, letting $\overline{p}_{i,j}^n = (\gamma - 1)(\overline{E}_{i,j}^n - \frac{1}{2}(\overline{m}_{i,j}^n)^2 / \overline{\rho}_{i,j}^n)$, is done in two steps:

a. First, regulate a small number $\varepsilon = \min_j \left\{10^{-13}, \overline{\rho}_{i,j}^n, \overline{p}_{i,j}^n\right\}$.

b. Then, ensure the density remains positive in each cell $C_{i,j}$. Within every $C_{i,j}$, replace $\rho_i(x)$ with

$$\hat{\rho}_{i,j}(x) = \theta_1(\rho_i(x) - \overline{\rho}_{i,j}^n) + \overline{\rho}_{i,j}^n, \tag{4.10}$$

where

$$\theta_1 = \min\left\{ \frac{\overline{\rho}_{i,j}^n - \varepsilon}{\overline{\rho}_{i,j}^n - \rho_{\min}}, 1 \right\}, \ \rho_{\min} = \min_{\alpha} \rho_i(\hat{x}_{i,j}^{\alpha}). \tag{4.11}$$

With the mentioned modifications, the cell average of $\hat{\rho}_{i,j}(x)$ over $C_{i,j}$ is still $\overline{\rho}_{i,j}^n$ and $\hat{\rho}_{i,j}(\hat{x}_{i,j}^{\alpha}) \geq \varepsilon$. Now set $\hat{\mathbf{q}}_{i,j}(x) = (\hat{\rho}_{i,j}(x), m_i(x), E_i(x))^T$.

c. Finally, ensure that the pressure remains positive in each cell $C_{i,j}$. Define

$$Q_{i,j} = \left\{\hat{\mathbf{q}}_{i,j}(\hat{x}^{\nu}_{i,j}),\ \nu = 1, \ldots, N\right\}. \tag{4.12}$$

For every $\mathbf{q} \in Q_{i,j}$, if $p(\mathbf{q}) < \varepsilon$, determine $s_{\mathbf{q}}$ by solving

$$p\big[(1 - s_{\mathbf{q}})\,\bar{w}^{n}_{i,j} + s_{\mathbf{q}}\,\mathbf{q}\big] = \varepsilon. \tag{4.13}$$

If $p(\mathbf{q}) \geq \varepsilon$, assign $s_{\mathbf{q}} = 1$. Next, compute the updated polynomial vector as

$$\tilde{\mathbf{q}}_{i,j}(x) = \theta_2\big(\hat{\mathbf{q}}_{i,j}(x) - \bar{w}^{n}_{i,j}\big) + \bar{w}^{n}_{i,j}, \tag{4.14}$$

where

$$\theta_2 = \min_{\mathbf{q} \in Q_{i,j}} s_{\mathbf{q}}. \tag{4.15}$$

5. Numerical examples

This section evaluates the performance of the proposed limiters when applied to high-order spectral volume schemes through a series of numerical experiments. In section 5.1, we first investigate the maximum-principle-preserving schemes in the context of scalar conservation laws. Then, in section 5.2, we present examples for the compressible Euler equations to examine their positivity-preserving capability. In all test cases, the local Lax–Friedrichs flux is adopted as the baseline first-order monotone flux. Unless otherwise specified, the SVs are partitioned using the Gauss–Lobatto points defined in Equation (2.22). For temporal integration, we employ the third-order Runge–Kutta method given in Equation (2.21), with the time step Δt selected small enough to ensure that spatial discretization errors dominate over temporal ones.

5.1. **Scalar conservation laws.** Comparisons between the SV schemes with and without the MPP limiter, denoted by MPP and Non-MPP respectively, are presented in the following examples in tabular or graphical form. The minimum and maximum numerical solutions of the SV scheme are denoted by $\bar{u}_{min}$ and $\bar{u}_{max}$.

Example 5.1. We consider the linear advection equation [30]

$$u_t + u_x = 0, \quad u(x, 0) = u_0(x), \tag{5.1}$$

subject to periodic boundary conditions on the interval $[-1, 1]$. To assess the accuracy of the high-order RK SV method combined with the MPP limiter, we choose a smooth initial profile

$$u_0(x) = \sin^4(\pi x).$$

The SVs are partitioned using the clustering points defined in (2.23) with parameter $\mu = 2.6$. We compute solutions at final time $T = 1$ using third-, fourth-, and fifth-order RK SV schemes, both with and without the MPP limiter. The L_1 and L_∞ errors, along with the corresponding convergence orders, are reported in Table 1. Additionally, the maximum and minimum cell averages, $\bar{u}_{\min}$ and $\bar{u}_{\max}$, produced by each scheme are also listed. From Table 1, it is evident that the inclusion of the MPP limiter guarantees strict compliance with condition (1.4) while maintaining the designed order of accuracy.

Example 5.2. We now examine equation (5.1) with a square-wave initial profile on the interval $[0, 1]$ under periodic boundary conditions [23]:

$$u_0(x) = \begin{cases} 1, & \frac{1}{4} \leq x \leq \frac{3}{4}, \\ 0, & \text{otherwise.} \end{cases} \tag{5.2}$$

In this test, the domain $[0, 1]$ is divided into thirty spectral volumes. Figure 1 presents the numerical results at time $T = 1$ obtained using second- through fourth-order SV schemes, both with and without the MPP limiter. Without the limiter, the computed solutions exceed the theoretical bounds, whereas applying the MPP limiter ensures that the results remain strictly within the range $[0, 1]$. Moreover, the MPP limiter not only enforces the admissible range but also suppresses spurious oscillations and produces sharper resolution near discontinuities. For comparison, Figure 1

also includes results from the CVTVDM SV scheme [24], demonstrating that the MPP SV approach yields noticeably crisper transitions than the CVTVDM SV method.

Example 5.3. In this example, we consider Burgers' equation

$$u_t + \left(\frac{u^2}{2}\right)_x = 0,$$

TABLE 1. Errors and orders for SV scheme with and without MPP limiter, for Example 5.1 with the clustering points (2.23) with $\mu = 2.6$.

Order		N	L_1 error	L_1 order	L_∞ error	L_∞ order	$\bar{u}_{\min}$	$\bar{u}_{\max}$
$k=3$	Non-MPP	10	6.73e-02		7.47e-02		0.02453292	0.87177772
		20	1.30e-02	2.37	1.33e-02	2.49	-0.0038517	0.92745706
		40	1.76e-03	2.89	1.71e-03	2.96	-0.0008285	0.98216634
		80	2.21e-04	2.99	2.14e-04	3.00	-0.0001181	0.99569083
		160	2.77e-05	3.00	2.73e-05	2.97	-0.0000154	0.99894619
		320	3.47e-06	3.00	3.45e-06	2.98	-0.0000020	0.99973970
	MPP	10	5.66e-02		4.41e-02		0.03454840	0.87221496
		20	1.04e-02	2.44	1.34e-02	2.47	0.00035028	0.92748916
		40	1.71e-03	2.60	1.72e-03	2.96	0.00000450	0.98216682
		80	2.22e-04	2.95	2.29e-04	2.91	0.00000060	0.99569040
		160	2.77e-05	3.00	3.18e-05	2.85	0.00000009	0.99894586
		320	3.47e-06	3.00	4.18e-06	2.93	0.00000000	0.99973949
$k=4$	Non-MPP	5	9.46e-02		1.03e-01		0.01988184	0.67467557
		10	1.26e-02	2.91	1.14e-02	3.17	0.02251894	0.92937077
		20	7.61e-04	4.05	7.06e-04	4.02	0.00137857	0.93727609
		40	4.58e-05	4.05	4.14e-05	4.09	0.00010017	0.98374920
		80	2.80e-06	4.03	2.59e-06	4.00	0.00000691	0.99590023
		160	1.74e-07	4.01	1.62e-07	4.00	0.00000045	0.99897271
	MPP	5	7.64e-02		1.04e-01		0.04765392	0.66542588
		10	9.22e-03	3.05	1.15e-02	3.18	0.02348970	0.92924633
		20	7.31e-04	3.66	8.72e-04	3.72	0.00144035	0.93723789
		40	4.63e-05	3.98	5.87e-05	3.89	0.00009907	0.98374447
		80	2.87e-06	4.01	3.31e-06	4.15	0.00000662	0.99589982
		160	1.79e-07	4.01	1.96e-07	4.08	0.00000043	0.99897269
$k=5$	Non-MPP	4	1.00e-01		8.80e-02		0.37366224	0.37633776
		8	4.45e-03	4.49	5.86e-03	3.91	0.05642309	0.69359753
		16	1.90e-04	4.55	1.87e-04	4.97	0.00433120	0.90463485
		32	5.83e-06	5.02	5.32e-06	5.13	0.00028804	0.97478287
		64	1.81e-07	5.01	1.57e-07	5.08	0.00001837	0.99360520
		128	5.69e-09	4.99	4.81e-09	5.03	0.00000116	0.99839555
	MPP	4	6.38e-02		8.98e-02		0.36803999	0.38196001
		8	3.65e-03	4.13	5.99e-03	3.91	0.05677892	0.69369266
		16	1.95e-04	4.23	1.87e-04	5.00	0.00431365	0.90463522
		32	5.82e-06	5.06	6.50e-06	4.85	0.00028710	0.97478285
		64	1.81e-07	5.00	2.29e-07	4.83	0.00001833	0.99360520
		128	5.69e-09	4.99	7.53e-09	4.93	0.00000115	0.99839555

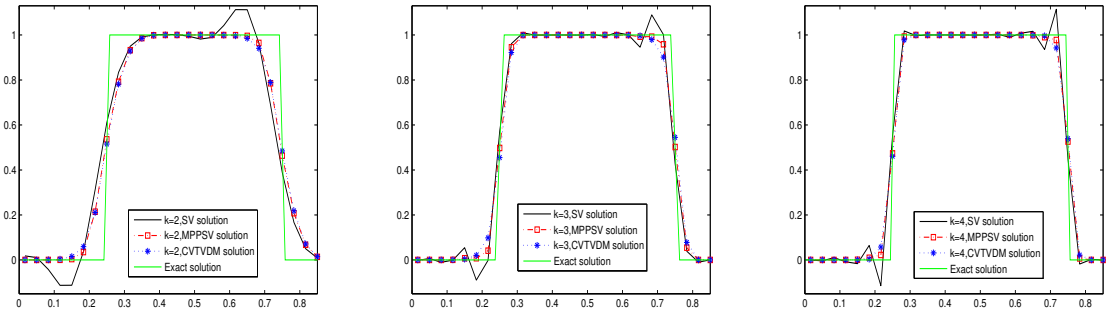

FIGURE 1. Numerical solutions of Equation (5.1) with square wave (5.2) at time $T = 1$ with 30 spectral volumes.

on the domain $[-1, 1]$ with periodic boundary conditions [23]. The initial condition is taken as

$$u_0(x) = 1 + \frac{1}{2}\sin(\pi x), \tag{5.3}$$

for which the exact solution remains smooth up to time $t = \frac{2}{\pi}$.

We perform computations at $T = 0.3$ using third- to fifth-order Runge–Kutta spectral volume schemes, both with and without the MPP limiter. The corresponding L_1 and L_∞ errors and convergence rates are presented in Table 2. It is evident that the RK SV schemes incorporating the MPP limiter (3.5) achieve the expected order of accuracy in both norms.

At time $t = \frac{2}{\pi}$, the solution begins to develop a shock, which becomes fully formed for $t > \frac{2}{\pi}$. We apply the third-order MPP RK SV method with $N = 50$ spectral volumes at $t = \frac{2}{\pi}$, and the numerical results are displayed in Figure 2. Without the limiter, the minimum and maximum cell averages of the RK SV solution are $\bar{u}_{\min} = 5.0033 \times 10^{-1}$ and $\bar{u}_{\max} = 1.4996$, indicating no overshoots or undershoots at this time. The figure illustrates that the scheme captures sharp solution features without spurious oscillations at the onset of shock formation.

Table 3 presents the maximum and minimum cell average values at $T = 1$ for the third-order RK SV scheme, both with and without the application of limiters. It is evident that, in the absence of limiters, the solution exhibits significant overshoots and undershoots. Conversely, when the MPP limiter is employed, these undesirable oscillations are effectively suppressed, with the cell averages remaining confined within the interval $\left[\frac{1}{2}, \frac{3}{2}\right]$. The impact of the MPP limiter is further demonstrated in Figure 3, which shows the numerical solution obtained using the third-order RK SV scheme with forty spectral volumes at $T = 1$, highlighting the reduction of overshoot and undershoot near shock and discontinuity.

Example 5.4. The one-dimensional Buckley–Leverett equation is given by

$$u_t + \frac{\partial}{\partial x} f(u) = 0, \quad x \in [-1, 1], \tag{5.4}$$

where the flux function is the nonconvex Buckley–Leverett flux

$$f(u) = \frac{4u^2}{4u^2 + (1-u)^2}. \tag{5.5}$$

The initial condition is prescribed as

$$u(x, 0) = \begin{cases} 1, & -0.5 \le x \le 0, \\ 0, & \text{otherwise.} \end{cases} \tag{5.6}$$

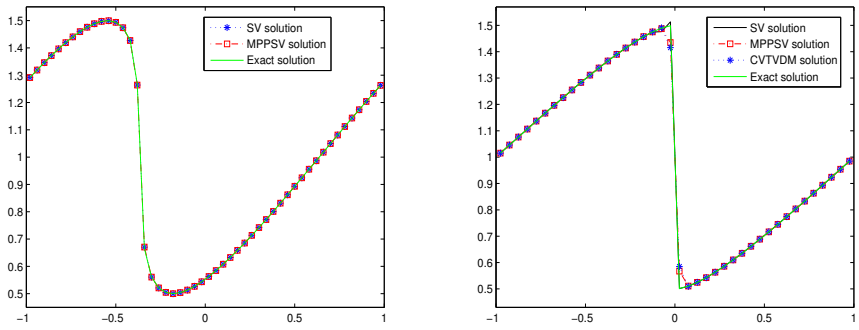

FIGURE 2. Numerical solutions of Burger's equation with initial function (5.3) at times $T = 0.3$ and $T = 1$, respectively with 40 spectral volumes.

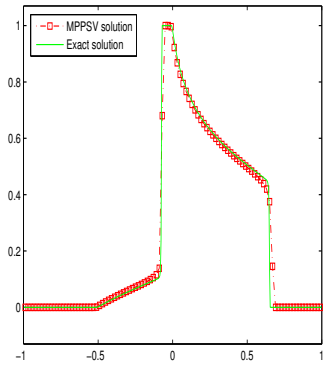

FIGURE 3. Numerical solutions of Buckley-Leverett equation with initial function (5.6) at time $T = 0.4$ with 100 spectral volumes.

The solution is computed up to time $T = 0.4$ under periodic boundary conditions. Table 4 summarizes the maximum and minimum values of the numerical solutions obtained using second- through fifth-order RK SV schemes. The results reveal that overshoots and undershoots occur when the MPP limiter is not applied, whereas these nonphysical oscillations are successfully eliminated upon incorporating the MPP limiter. The computational results of fourth order RK SV scheme using $N = 100$ spectral volumes at $T = 0.4$ are displayed in Figure 3. The exact solution is obtained from the high order WENO scheme on a very fine mesh. We can observe that the fifth order RK SV scheme with the limiter can produce high resolution and non-oscillatory numerical solutions. From the SV scheme without limiter, we obtain the maximum and minimum of the numerical solutions to be 1.00011633041 and -0.00004485179 respectively, while by the SV scheme with limiter, the maximum and minimum of the numerical solutions are exactly 0 and 1 the same as indicated by the initial conditions.

5.2. **Compressible Euler equation.** To show that PP SV scheme can preserve the positivity of numerical solution of compressible Euler equation, we choose three problems here. The parameter γ is taken to be 1.4 for all tests.

Example 5.5. In the first one, we use the Euler equation with initial conditions[34] $\rho(x, 0) = 7$, $p(x, 0) = 0.2$ and $u(x, 0)$ is a piecewise constant state with a jump at $\alpha = 0$, where, $u_l = -1$, $u_r = 1$. It contains double rarefaction waves. In this test, the computational domain $[-1, 1]$ is divided into 400 spectral volumes. Figure 1 shows the curves

TABLE 2. Errors and orders for SV scheme with/without MPP flux limiter, for Example 5.3 with GL-nodes.

Order		N	L_1 error	L_1 order	L_∞ error	L_∞ order	$\bar{u}_{\min}$	$\bar{u}_{\max}$
$k=3$	Non-MPP	10	1.92e-03		6.50e-03		0.51245644	1.48787860
		20	2.56e-04	2.90	1.34e-03	2.28	0.50205745	1.49796750
		40	3.33e-05	2.95	2.23e-04	2.58	0.50194727	1.49805308
		80	4.19e-06	2.99	3.14e-05	2.83	0.50050011	1.49949989
		160	5.33e-07	2.97	4.12e-06	2.93	0.50012675	1.49987325
		320	6.73e-08	2.99	5.27e-07	2.97	0.50003191	1.49996809
	MPP	10	1.89e-03		6.50e-03		0.51252773	1.48754854
		20	2.54e-04	2.90	1.34e-03	2.28	0.50208041	1.49791238
		40	3.35e-05	2.92	2.23e-04	2.58	0.50194350	1.49804549
		80	4.31e-06	2.96	3.14e-05	2.83	0.50049923	1.49949684
		160	5.65e-07	2.93	4.12e-06	2.93	0.50012657	1.49987209
		320	7.52e-08	2.91	5.27e-07	2.97	0.50003187	1.49996781
$k=4$	Non-MPP	5	2.44e-03		8.66e-03		0.54932844	1.43670494
		10	1.52e-04	4.00	8.35e-04	3.38	0.51242525	1.48756261
		20	1.79e-05	3.09	1.59e-04	2.39	0.50206198	1.49793665
		40	1.11e-06	4.01	1.21e-05	3.72	0.50194767	1.49805229
		80	7.06e-08	3.97	8.07e-07	3.90	0.50050013	1.49949986
		160	4.50e-09	3.97	5.37e-08	3.91	0.50012675	1.49987325
	MPP	5	2.37e-03		8.91e-03		0.54936960	1.43654967
		10	1.53e-04	3.95	8.35e-04	3.42	0.51242512	1.48755779
		20	1.80e-05	3.09	1.59e-04	2.39	0.50206211	1.49793596
		40	1.11e-06	4.02	1.21e-05	3.72	0.50194766	1.49805222
		80	7.20e-08	3.94	8.07e-07	3.90	0.50050013	1.49949984
		160	4.76e-09	3.92	5.37e-08	3.91	0.50012675	1.49987324
$k=5$	Non-MPP	4	2.50e-03		1.09e-02		0.55720671	1.40087396
		8	8.90e-05	4.81	5.24e-04	4.38	0.51623477	1.47807760
		16	4.94e-06	4.17	5.25e-05	3.32	0.50602411	1.49656819
		32	1.47e-07	5.07	3.13e-06	4.07	0.50087762	1.49823347
		64	5.03e-09	4.87	1.11e-07	4.81	0.50042933	1.49977213
		128	1.64e-10	4.94	3.65e-09	4.93	0.50005659	1.49989699
	MPP	4	2.50e-03		1.09e-02		0.55720570	1.40084810
		8	9.00e-05	4.80	5.40e-04	4.34	0.51623485	1.47807435
		16	4.94e-06	4.18	5.25e-05	3.37	0.50602412	1.49656813
		32	1.47e-07	5.07	3.13e-06	4.07	0.50087762	1.49823347
		64	5.08e-09	4.85	1.11e-07	4.81	0.50042933	1. 49977213
		128	1.69e-10	4.91	3.65e-09	4.93	0.50005659	1.49989699

of the density, velocity, pressure and energy at $T = 0.18$. We can observe that fourth order RK SV schemes with the positivity preserving limiter produce strictly positive solutions.

Example 5.6. The second one is Sod's Shock Tube problem with the initial condition[22] $u(x,0) = 0$ and $\rho(x,0), p(x,0)$ are picewise constant with a jump at $\alpha = 0.5$. where, $\rho_l = 1$, $\rho_r = 0.125$, $p_l = 1$ and $p_r = 0.1$. It is evolved in the

TABLE 3. Max/Min cell averages for Burger's equation with GL-nodes at $T = 1$.

Order		Non-MPP		MPP	
$k = 3$	N	$\bar{u}_{min}$	$\bar{u}_{max}$	$\bar{u}_{min}$	$\bar{u}_{max}$
	10	0.51437096087	1.50267962429	0.57812174623	1.42412341390
	20	0.50320386975	1.51440022019	0.53435901300	1.46402758414
	40	0.50125583445	1.51309536258	0.51069689911	1.48713349504
	80	0.50011917341	1.51398168263	0.50306977042	1.49498043589
	160	0.49982230505	1.51418950464	0.50082980175	1.49786640654
	320	0.49974337521	1.51424636958	0.50021484186	1.49942956224

TABLE 4. Max/Min cell averages for Buckley-Leverett equation with GL-nodes subdivided $N = 100$ at $T = 0.4$.

Order	Non-MPP		MPP	
	$\bar{u}_{min}$	$\bar{u}_{max}$	$\bar{u}_{min}$	$\bar{u}_{max}$
$k = 2$	-0.00235073880	1.00488881933	0	1
$k = 3$	-0.00003201803	0.99978555727	0	1
$k = 4$	-0.00004485179	1.00011633041	0	1
$k = 5$	-0.00003714247	0.99998514632	0	1

computational domain $[-6, 6]$ with periodic boundary conditions until $T = 1$. The exact solution of this problem contains a rarefaction wave, a contact discontinuity and a shock wave. The numerical results of fourth order RK SV scheme with positivity preserving limiter using $N = 100$ SVs are plotted in Figure 5. As can be seen, the RK SV scheme with limiter can produce high resolution results with out numerical oscillations that the primitive variables, density and pressure, are strictly positive.

Example 5.7. The last one is Lax shock tube problem [11], where the initial conditions are piecewise constant with a jump at $\alpha = 0.5$ and $\rho_l = 0.445$, $\rho_r = 0.5$, $p_l = 3.528$, $p_r = 0.571$, $u_l = 0.698$ and $u_r = 0$. The exact solutions of this system consist of a rarefaction wave, a contact discontinuity and a shock wave. Computing the numerical approximation of this system with parameters $N = 100$ and $T = 0.16$ on the domain $[0, 1]$ yields the visible results in the Figure 6. The curves refer to the results obtained from positivity preserving fourth order SV scheme. In fact without positivity preserving limiter, The code violates due to the failure of convergence of the nonlinear solver. Practically, the positivity preserving limiter adds stability to the nonlinear solver.

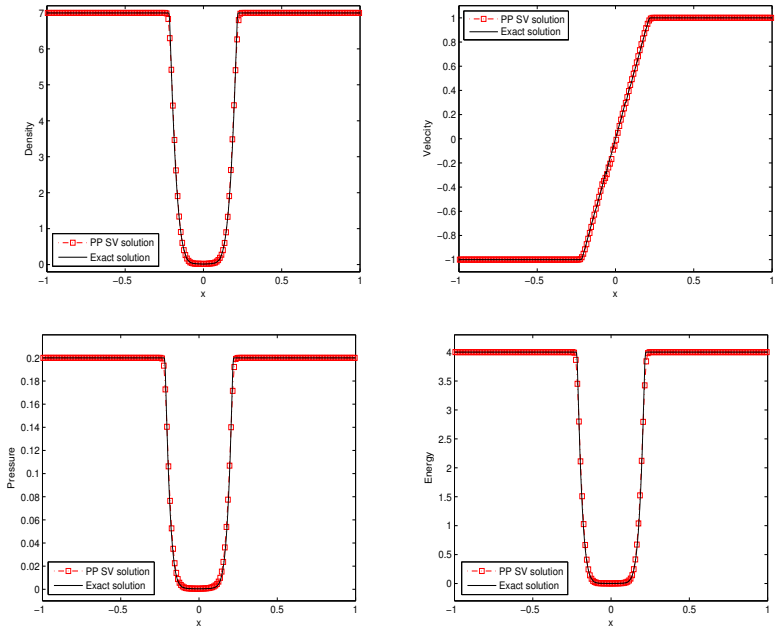

FIGURE 4. Simulation of double rarefaction problem at time $T = 0.18$ with $N = 200$.

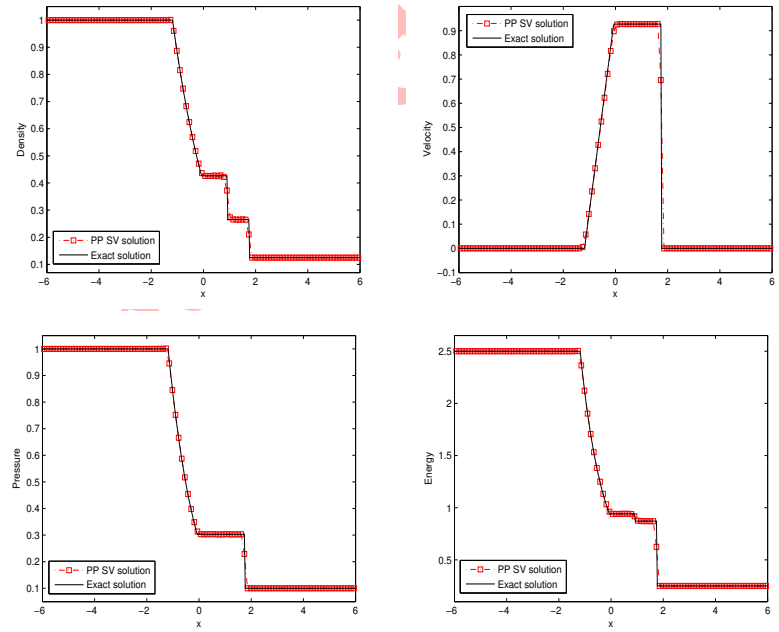

FIGURE 5. Simulation of Sod's Shock Tube problem at time $T = 1$ with $N = 100$.

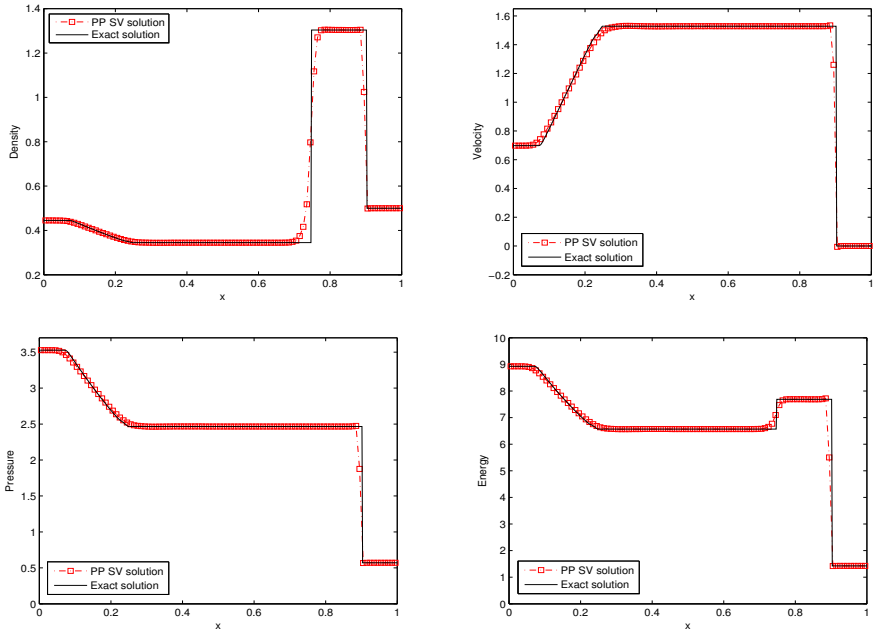

FIGURE 6. Simulation of Lax shock tube problem at time $T = 0.16$ with $N = 100$.

6. Conclusion

In this paper, we present high order accurate maximum-principle-satisfying spectral volume scheme for hyperbolic conservation laws. Via careful theoretical analysis and extensive numerical tests, we show that under an appropriate CFL condition And by applying a simple scaling limiter on the reconstruction, we can construct high order SV scheme that maintains the maximum principle. Our results indicate that the SV scheme with reconstruction-limiting function can be regarded as a structurally simple algorithm that is conventionally applicable to the numerical solution of equations. The advantages of MPP SV scheme are that it maitain high order of accuracy in smooth regions and resolves discontinuities uniformly with a sharper conduction.

References

[1] T. Barth and P. Frederickson, *High-order solution of the Euler equations on unstructured grids using quadratic reconstruction,* 28th Aerospace Sciences Meeting, 1990.

[2] A. J. Christlieb, Y. Liu, Q. Tang, and Z. Xu, *High order parametrized maximum-principle-preserving and positivity-preserving WENO schemes on unstructured meshes*, Journal of Computational Physics, *281* (2015), 334–351.

[3] A. J. Christlieb, X. Feng, D. C. Seal, and Q. Tang, *A high-order positivity-preserving single-stage single-step method for the ideal magnetohydrodynamic equations,* Journal of Computational Physics, *316* (2016), 218–242.

[4] B. Cockburn and C. W. Shu, *The Runge–Kutta local projection P^1-discontinuous Galerkin finite element method for scalar conservation laws*, Mathematical Modelling and Numerical Analysis, *25*(3) (1991), 337–361.

[5] M. Crandall and A. Majda, *Monotone difference approximations for scalar conservation laws,* Mathematics of Computation, *34* (1980), 1–21.

[6] N. R. Gande, Y. Rathod, and S. Rathan. *Third-order WENO scheme with a new smoothness indicator,* Int. J. Numer. Methods Fluids, *85*(2) (2017), 90–112.

[7] J. L. Guermond, M. Nazarov, B. Popov, and Y. Yang, *Invariant domains and second-order continuous finite element approximation for scalar conservation equations*, SIAM Journal on Numerical Analysis, *55*(6) (2017), 3120–3146.
[8] Y. Guo, T. Xiong, and Y. Shi, *A positivity-preserving high order finite volume compact-WENO scheme for compressible Euler equations*, Journal of Computational Physics, *274* (2014), 505–523.
[9] C. Hu and C. W. Shu, *Weighted essentially non-oscillatory schemes on triangular meshes*, Journal of Computational Physics, *150*(1) (1999), 97–127.
[10] G. S. Jiang and E. Tadmor, *Non-oscillatory central schemes for multidimensional hyperbolic conservative laws*, SIAM Journal on Scientific Computing, *19* (1998), 1892–1917.
[11] P. D. Lax, *Weak solutions of nonlinear hyperbolic equations and their numerical computation,* Comm. Pure Appl. Math., *7*(1) (1954), 159–193.
[12] C. Liang and Z. Xu, *Parametrized maximum principle preserving flux limiters for high order schemes solving multi-dimensional scalar hyperbolic conservation laws*, Journal of Scientific Computing, *58*(1) (2014), 41–60.
[13] M. Li, F. Li, Z. Li, and L. Xu, *Maximum-Principle-Satisfying and Positivity-Preserving High Order Central Discontinuous Galerkin Methods for Hyperbolic Conservation Laws*, SIAM J. Sci. Comput., *38*(6) (2016), A3720–A3740.
[14] X. D. Liu, S. Osher, *Non-oscillatory high order accurate self similar maximum principle satisfying shock capturing schemes*, SIAM J. Numer. Anal., *33* (1996), 760–779.
[15] S. Mousavi Yeganeh and J. Farzi, *Maximum principle and positivity-preserving high order spectral volume schemes with parametrized flux limiters for solving hyperbolic conservation laws*, Journal of Computational and Applied Mathematics, *404* (2022), 113893.
[16] B. Perthame and C. W. Shu, *On positivity preserving finite volume schemes for Euler equations*, Numerische Mathematik, *73*(1) (1996), 119–130.
[17] T. Qin, C. W. Shu, and Y. Yang, *Bound-preserving discontinuous Galerkin methods for relativistic hydrodynamics,* Journal of Computational Physics, *315* (2016), 323–347.
[18] D. C. Seal, Q. Tang, Z. Xu, and A. J. Christlieb, *An explicit high-order single-stage single-step positivity-preserving finite difference WENO method for the compressible Euler equations,* Journal of Scientific Computing, *68*(1) (2016), 171–190.
[19] Y. Shi and Y. Guo, *A maximum-principle-satisfying finite volume compact-WENO scheme for traffic flow model on networks.* Applied Numerical Mathematics, *108* (2016), 21–36.
[20] C. W. Shu, *Total-variation-diminishing time discretizations,* SIAM J. Sci. Stat. Comput., *9*(6) (1988), 1073–1084.
[21] C. W. Shu, *Essentially non-oscillatory and weighted essentially non-oscillatory schemes for hyperbolic conservation laws*, in Advanced Numerical Approximation of Nonlinear Hyperbolic Equations, edited by A. Quarteroni, Lecture Notes in Mathematics (Springer, 1998), Vol. 1697, p. 325.
[22] G. A. Sod, *A Survey of Several Finite Difference Methods for Systems of Nonlinear Hyperbolic Conservation Laws,* Journal of Computational Physics, *27*(1) (1978), 1–31.
[23] Z. Wang, *Spectral (finite) volume method for conservation laws on unstructured grids: Basic formulation*, Journal of Computational Physics, *178*(1) (2002), 210–251.
[24] Z. J. Wang and L. Yen, *Spectral (finite) volume method for conservation laws on unstructured grids II. Extension to two-dimensional scalar equation*, Journal of Computational Physics, *179*(2) (2002), 665–697.
[25] T. Xiong, J. Qiu, and Z. Xu, *A parametrized maximum principle preserving flux limiter for finite difference RK-WENO schemes with applications in incompressible flows*, Journal of Computational Physics, *252* (2013), 310–331.
[26] T. Xiong, J. Qiu, and Z. Xu, *High order maximum-principle-preserving discontinuous Galerkin method for convection-diffusion equations*, SIAM Journal on Scientific Computing, *37*(2) (2015), A583–A608.
[27] T. Xiong, J. Qiu, and Z. Xu, *Maximum-principle-preserving discontinuous Galerkin method for convection-diffusion equations*, SIAM Journal on Scientific Computing, *37*(2) (2015), 583–608.
[28] Z. Xu, *Parametrized maximum principle preserving flux limiters for high order schemes solving hyperbolic conservation laws: one-dimensional scaler problem*, Mathematics of Computation, *83*(289) (2014), 2213–2238.

[29] P. Yang, T. Xiong, J. Qiu, and Z. Xu, *High order maximum principle preserving flux finite volume method for convection dominated problems*, Journal of Scientific Computing, *67* (2015), 795–820.
[30] X. Zhang and C. W. Shu, *On maximum-principle-satisfying high order schemes for scalar conservation laws*, Journal of Computational Physics, *229* (2010), 3091–3120.
[31] X. Zhang, Y. Xia, and C. W. Shu, *Maximum-principle-satisfying and positivity-preserving high order discontinuous Galerkin schemes for conservation laws on triangular meshes*, Journal of Scientific Computing, *50*(1) (2012), 29–62.
[32] Y. Zhang, X. Zhang, and C. W. Shu, *Maximum-principle-satisfying second order discontinuous Galerkin schemes for convection–diffusion equations on triangular meshes.* Journal of Computational Physics, *234* (2013), 295–316.
[33] X. Zhang and C. W. Shu, *Positivity-preserving high order discontinuous Galerkin schemes for compressible Euler equations with source terms,* Journal of Computational Physics, *230* (2011), 1238–1248.
[34] X. Zhang, *On positivity-preserving high order discontinuous Galerkin schemes for compressible Navier-Stokes equations,* Journal of Computational Physics, *328* (2017), 301–343.